BIOCHEMISTRY
including biophysical chemistry & molecular biology
Article

Biochemistry **2010,** *49,* 4483–4493 4483
DOI: 10.1021/bi902201y

Quantitative Analysis of VirB8−VirB9−VirB10 Interactions Provides a Dynamic Model of Type IV Secretion System Core Complex Assembly†

Durga Sivanesan,‡,∥ Mark A. Hancock,§ Ana María Villamil Giraldo,∥ and Christian Baron*,‡,∥

‡*Department of Biology, McMaster University, 1280 Main Street West, Hamilton, ON L8S 4K1, Canada,* §*Sheldon Biotechnology Centre, McGill University, 3773 University Street, Montréal, QC H3A 2B4, Canada, and* ∥*Département de biochimie, Université de Montréal, C.P. 6128, Succ. Centre-ville, Montréal, QC H3C 3J7, Canada*

Received December 23, 2009; Revised Manuscript Received April 27, 2010

ABSTRACT: Type IV secretion systems are multiprotein complexes that translocate macromolecules across the bacterial cell envelope. The type IV secretion system in *Brucella* species encodes 12 VirB proteins that permit this pathogen to translocate effectors into mammalian cells, where they contribute to its survival inside the host. The "core" complex proteins are conserved in all type IV secretion systems, and they are believed to form the channel for substrate translocation. We have investigated the in vitro interactions between the soluble periplasmic domains of three of these VirB components, VirB8, VirB9, and VirB10, using enzyme-linked immunosorbent assays, circular dichroism, and surface plasmon resonance techniques. The in vitro experiments helped in the quantification of the self-association and binary interactions of VirB8, VirB9, and VirB10. Individually, distinct binding properties were revealed that may explain their biological functions, and collectively, we provide direct evidence of the in vitro formation of the VirB8−VirB9−VirB10 ternary complex. To assess the dynamics of these interactions in a simplified in vivo model of complex assembly, we applied the bacterial two-hybrid system in studying interactions between the full-length proteins. This approach demonstrated that VirB9 stimulates the self-association of VirB8 but inhibits VirB10−VirB10 and VirB8−VirB10 interaction. Analysis of a dimerization site variant of VirB8 ($VirB8^{M102R}$) suggested that the interactions with VirB9 and VirB10 are independent of its self-association, which stabilizes VirB8 in this model assay. We propose a dynamic model for secretion system assembly in which VirB8 plays a role as an assembly factor that is not closely associated with the functional core complex comprising VirB9 and VirB10.

T4SS[1] are essential virulence factors in many Gram-negative pathogens (*1*−*5*). The association between 8 and 12 VirB proteins generates a macromolecular complex that spans the inner and outer membrane of Gram-negative bacteria, and this complex mediates translocation of the substrate across the cell envelope (*5*). T4SS serve different functions that are specifically adapted to the needs of individual organisms. In the well-studied plant pathogen *Agrobacterium tumefaciens*, two T4SS serve as conjugation machineries that transfer plasmid DNA between bacterial cells, and the third one transfers the tumor-inducing DNA (T-DNA) into plant cells (*6*). In *Brucella* species, the causal agents of brucellosis in humans and animals, the T4SS transfers effector proteins to evade the host immune system and facilitate replication in mammalian cells (*7*−*9*). Regardless of the functional differences between the two pathogens, *A. tumefaciens* and *Brucella*, the *virB* operon structures are similar and the gene products are significantly similar in sequence (*10*). However, the T4SS of *Brucella* does not appear to contain a homologue of VirD4, a coupling protein that targets T-DNA to the *Agrobacterium* VirB components (*11*, *12*), but the operon encodes an additional VirB component, the VirB12 protein. It was shown that VirB2−VirB11 are essential for virulence in the *A. tumefaciens* model, whereas VirB12 is not essential for *Brucella* virulence (*13*−*15*). Most T4SS comprise a VirB1 homologue, a lytic transglycosylase that is believed to facilitate complex assembly by degrading the peptidoglycan in the periplasm (*16*, *17*). The T4SS proteins are grouped into three categories: energizers (VirB4, VirB11, and VirD4) that predominately localize in the cytoplasm but also associate with the inner membrane, core components (VirB6−VirB10) that are believed to form a conduit from the inner to the outer membrane, and pilus assembly components (VirB2, VirB3, and VirB5) that mediate the assembly of the extracellular pilus comprised of VirB2 and VirB5 (*5*, *12*, *18*, *19*).

A major challenge in the T4SS field is to determine the sequence in which VirB proteins assemble into a functional complex in the membranes of Gram-negative bacteria. Working with *Brucella* species requires level three biohazard containment, which constitutes a major constraint that prevents extensive biochemical experimentation (e.g., large-scale growth, extraction, and protein analysis) of the T4SS from this organism. To circumvent these constraints, we previously expressed the *Brucella suis* VirB proteins in the heterologous host *A. tumefaciens* and showed via cross-linking and immunofluorescence analysis that the core complex structure was qualitatively similar to that of the T4SS from other bacteria (*20*). In addition, different approaches such as detergent extraction of the membrane proteins,

†This work was supported by grants to C.B. from the Canadian Institutes of Health Research (CIHR Grants MOP-64300 and MOP-84239), the Hans Selye Research Chair (Bristol-Myers Squibb), the Canada Foundation for Innovation, and the Ontario Innovation Trust. Sheldon Biotechnology Centre is supported by a Research Resource Grant from the CIHR.

*To whom correspondence should be addressed. Telephone: (514) 343-6372. Fax: (514) 343-2210. E-mail: christian.baron@umontreal.ca.

[1]Abbreviations: AC, adenylate cyclase; AUC, analytical ultracentrifugation; BTH, bacterial two-hybrid; cAMP, cyclic adenosine monophosphate; CD, circular dichroism; ELISA, enzyme-linked immunosorbent assay; ONPG, *o*-2-nitrophenyl β-D-galactopyranoside; RU, resonance unit; SPR, surface plasmon resonance; T4SS, type IV secretion system(s).

Published on Web 04/28/2010

yeast two-hybrid analysis, cross-linking, and pull down studies in the model organism *A. tumefaciens* provided a working model of T4SS assembly (*21*−*24*). These studies provided mostly qualitative and static insights into core complex assembly, and quantitative analyses of protein interaction are required to gain insights into the dynamics and sequence of complex assembly (*25*, *26*).

To quantitatively analyze T4SS assembly, we here characterize formation of a complex of *B. suis* VirB8, VirB9, and VirB10. VirB8 and VirB10 are bitopic inner membrane proteins. The N-termini comprise short cytoplasmic domains, followed by a single transmembrane region and a large C-terminal periplasmic domain that determines the key protein functions (*24*). Recently, it was shown that VirB10 inserts into the outer membrane as well as into the inner membrane (*27*). VirB9 is a periplasmic protein that contains a signal sequence and localizes in the outer membrane where it forms a complex with the small lipoprotein VirB7 (*28*−*35*). All three proteins are essential for T4SS assembly and function (*36*−*44*), and binary interactions among VirB8, VirB9, and VirB10 were previously reported (*22*, *24*, *37*, *41*, *45*, *46*). Despite the finding that VirB8 did not co-immunoprecipitate with VirB9 and VirB10 from *A. tumefaciens* (*32*) and that it was not part of the VirB7−VirB9−VirB10 core complex recently described by cryo-electron microscopy (cryo-EM) and crystallographic analysis (*18*, *27*), the fact that it interacts with many proteins in vitro and in the yeast two-hybrid system suggests that VirB8, VirB9, and VirB10 form at least a transient complex.

In this report, we provide qualitative and quantitative results that provide novel insights into T4SS core complex assembly, notably into the role of VirB8. Using ELISA, CD spectroscopy, SPR, and BTH assays, we assessed self-associations and binary interactions among VirB8, VirB9, and VirB10. Furthermore, we provide direct evidence of the formation of a ternary complex of VirB8, VirB9, and VirB10 leading to a dynamic model for their assembly into the core complex.

EXPERIMENTAL PROCEDURES

Growth of Bacterial Strains and Construction of Plasmids. All *Escherichia coli* strains were grown in LB medium (1% tryptone, 0.5% yeast extract, and 1% NaCl) at 37 °C unless otherwise stated in subsequent procedures. The strains and plasmids used in this study are listed in Table 1 of the Supporting Information. For propagation of pT7-7strepII and pUT18C constructs, carbenicillin was added to the medium at a concentration of 100 μg/mL, whereas for the propagation of pKT25 constructs, 50 μg/mL kanamycin was added. All cloning experiments were conducted according to standard procedures (*47*). We constructed the bicistronic plasmids for the bacterial two-hybrid (BTH) assays by first eliminating the single *Hin*dIII restriction site in the gene encoding the T18 fragment of adenylate cyclase in pUT18CB8. To this end, we created a silent mutation using inverse polymerase chain reaction (PCR) with 5HIN and 3HIN primers to produce the construct pUT18CB8HIN, and this permitted the cloning of Shine-Dalgarno (SD) and *virB* genes downstream of the first *virB* gene. The primers used for PCRs are listed in Table 2 of the Supporting Information. For cloning of the genes downstream of the pUT18-encoded *virB8* gene, two oligonucleotides (5LNH and 3LNH) carrying unique restriction sites (*Nco*I and *Hin*dIII) and a SD sequence to ensure gene expression were synthesized. The annealed oligonucleotides were cloned into the *Kpn*I and *Eco*RI restriction sites downstream of *virB8* in pUT18CB8HIN to create pUT18CB8+SD. Next, the *virB9* and *virB10* fragments were PCR amplified from a template containing the *virB* operon of *B. suis* (pTrc200B1+3-12) (*20*) using primers listed in Table 2 of the Supporting Information and were subcloned into pUT18CB8+SD to create pUT18CB8+B9 and pUT18CB8+B10. Finally, the SD sequence along with the *virB9* and *virB10* genes from pUT18CB8+B9 and pUT18CB8+B10 was subcloned into pUT18CB10 to create pUT18CB10+B9 and pUT18CB10+B10, respectively. Variant VirB8^{M102R} was subcloned into pKT25 and pUT18C to create pKT25B8^{M102R} and pUT18CB8^{M102R}, respectively, by using PCR primers that are described elsewhere (*48*). The pUT18CB8^{M102R} construct was used to subclone the SD sequence along with the *virB9* gene from pUT18CB8+B9 to create pUT18CB8^{M102R}+B9.

Overproduction and Purification of Proteins. Derivatives of plasmid pT7-7strepII expressing the periplasmic portions of VirB8, VirB9, and VirB10 were electroporated into *E. coli* BL21-star (λDE3) for overproduction and purification. The BL21star (λDE3) cells expressing the *virB* genes were grown at 37 °C under aerobic conditions to an optical density (A_{600}) of 0.4−0.8, induced for T7 expression by addition of 0.5 mM IPTG, and further cultivated for 16 h at 26 °C. The cells were then harvested, lysed in a French press, and purified using strep-tactin Sepharose affinity chromatography as described previously (*23*). In the case of strepIIVirB8 and strepIIVirB8^{M102R}, the eluted proteins were subsequently purified using size exclusion chromatography (Superdex 75, Amersham Biosciences) at a flow rate of 0.5 mL/min in buffer A [100 mM Tris-HCl (pH 8), 150 mM NaCl, and 1 mM EDTA]. StrepIIVirB9 and strepIIVirB10 proteins eluted from the strep-tactin affinity column were further purified using ion exchange chromatography at a flow rate of 1 mL/min. For VirB9, the affinity-purified fractions were first dialyzed into 20 mM Tris-HCl (pH 6.8) for 12 h at 4 °C, followed by CM Sepharose fast flow cation exchange chromatography. The column was washed with buffer B [20 mM Tris-HCl (pH 6.8)], followed by elution with buffer C (buffer B with 1 M NaCl). For VirB10, the affinity-purified fractions were first dialyzed into 20 mM Tris-HCl (pH 8) for 12 h at 4 °C, followed by Q-Sepharose fast flow anion exchange chromatography using buffers B and C at pH 8. After elution, the purified proteins were dialyzed extensively against HBS [10 mM Hepes (pH 7.5), 150 mM NaCl, and 3 mM EDTA] at 4 °C and the final concentrations were determined with a Bradford assay using the Bio-Rad protein reagent (Bio-Rad, Hercules, CA) with BSA as the standard. The molecular weight and purity of the proteins were verified by SDS−PAGE followed by Coomassie blue and silver staining.

Enzyme-Linked Immunosorbent Assay. For ELISAs, 50 μL of strepIIVirB8, strepIIVirB10, and BSA [10 μg/mL each in 100 mM sodium carbonate buffer (pH 9.6)] was coated to microtiter wells of Immuno 96 Microwell plates (NUNC) for 12 h at 4 °C. Multiwell plates were then washed with HBS-EP [10 mM Hepes (pH 7.5), 150 mM NaCl, 3 mM EDTA, and 0.005% Tween 20] to remove noncoated protein and then blocked with a 3% skim milk solution (200 μL/well in HBS-EP) to inhibit nonspecific binding. For dose−response experiments, strepIIVirB9 and strepIIVirB10 (0, 25, 50, and 100 pmol in a 3% skim milk solution) were added to the wells (final volume of 100 μL) and incubated for 2 h at room temperature. Next, the wells were washed twice (200 μL each) with HBS-EP, followed by the addition of VirB9- or VirB10-specific antiserum (1:10000 dilution; 100 μL/well) for 2 h at room temperature. The wells were then washed twice and incubated with HRP-conjugated goat anti-rabbit IgG (1:3000 dilution, 100 μL/well) for 2 h at room temperature.

The binding of antibody corresponding to bound protein was assessed by color development using 100 μL of a chromogenic solution (Research & Development Systems, Minneapolis, MN); the reaction was stopped by the addition of 50 μL of 0.5 M H_2SO_4, and color development was measured at 450 nm. The A_{540} value was subtracted to correct for the plate background according to the supplier's description (Research & Development Systems). For dissociation experiments, 150 mM to 1 M NaCl was included in sample incubations. In all experiments, controls were used, for instance, incubating the test proteins alone in the microtiter wells to account for background protein attachment, and the primary antisera were tested for cross-reactivity to the bound protein in the wells.

Circular Dichroism Spectroscopy. For CD assays, purified strepII-tagged VirB8, VirB9, and VirB10 were dialyzed into 10 mM sodium phosphate buffer (pH 7.5) containing 100 mM NaCl and 1 mM EDTA at 4 °C for 12 h. Far-UV wavelength scans (from 260 to 195 nm) of 1250 pmol of each protein alone and in combination were conducted using an AVIV spectropolarimeter with the temperature held at 25 °C in a 1 mm path length cell, a time constant of 1 s, and a bandwidth of 1 nm. Melting curves of the purified proteins alone and of mixtures were recorded from 25 to 95 °C (measurements at 222 nm at every step of 5 °C). The spectra obtained from the far-UV CD measurements and the temperature scans were corrected by subtraction of the signal obtained from parallel measurements with buffer alone. The measured ellipticity of the protein was converted to the mean residue ellipticity (degress per square centimeter per decimole) using the molar extinction coefficients of strepIIVirB8 (37820 cm^{-1} M^{-1}), strepIIVirB9 (37820 cm^{-1} M^{-1}), and strepIIVirB10 (28010 cm^{-1} M^{-1}), the total number of residues, and the concentration of the sample for analysis of secondary structure content. Averages of the mean residue ellipticities (MRE) from the individual proteins were used for conversion of the ellipticity from protein mixtures for analysis of secondary structure content. The quantification of secondary structures was performed by taking the average that was calculated by SELCON and CONTINILL, which were downloaded from the software package CDPro available at http://lamar.colostate.edu/~sreeram/CDPro (*49*). The quantification was performed as described previously (*50*).

Surface Plasmon Resonance. For SPR assays, the interactions between the purified strepII-tagged periplasmic domains of VirB8 (~20 kDa), VirB8^{M102R} (~20 kDa), VirB9 (~31 kDa), and VirB10 (~48 kDa) were examined using a BIACORE 3000 system (GE Healthcare Bio-Sciences AB, Uppsala, Sweden; BIAcontrol version 4.1 operating software). Experiments were performed on research-grade CM4 sensor chips (Biacore) at 25 °C using filtered (0.2 μm) and degassed ELISA buffer {HBS-EP [10 mM Hepes (pH 7.4), 150 mM NaCl, 3 mM EDTA, and 0.005% (v/v) Tween 20]}. Immobilized VirB surfaces [10 μg/mL in 10 mM sodium acetate (pH 4.0), final concentration of ~900 resonance units (RU)] were prepared using the Biacore Amine Coupling Kit as recommended by the manufacturer; corresponding reference surfaces were prepared in the absence of VirB proteins. Protein-grade detergents (Tween 20 and Empigen) were from Anatrace (Maumee, OH). Fatty acid-free bovine serum albumin (BSA) was purchased from Millipore (Billerica, MA). ImmunoPure Gentle Ag/Ab Elution Buffer was from Pierce (Rockford, IL). All other chemicals were reagent grade quality. To assess binding specificity and kinetics, equilibrium analyses were performed in which VirB proteins were titrated (0−25 μM VirB8, 0−5 μM VirB9, 0−5 μM VirB10, 0−25 μM BSA as a negative control) over VirB immobilized and reference surfaces at 5 μL/min using the "KINJECT" mode (10−20 min association, 10−20 min dissociation). For each titration series, a buffer blank was injected first, the highest analyte concentration second, and serial dilutions followed (from the lowest to the highest concentration). Comparing binding responses between the duplicated injections of the highest analyte injections verified consistent immobilized VirB surface activity throughout each assay. To determine if a single-point mutation (M102R) affects VirB8 self-association, wild-type and variant VirB8 (0−50 μM) were also titrated over immobilized VirB8 and VirB8^{M102R} surfaces as described above (including 0−50 μM BSA as a negative control). In all cases, the surfaces were regenerated between sample injections at 50 μL/min using two 30 s pulses of solution I [Pierce Gentle Elution containing 0.05% (v/v) Empigen] and solution II [HBS-EP containing 0.5 M NaCl, 50 mM EDTA, 5 mM NaOH, 0.05% (v/v) Tween 20, and 0.05% (v/v) Empigen], followed by the "EXTRACLEAN" and "RINSE" procedures. Because of the equilibrium style of analysis, binding responses were independent of mass transport limitations and all double-reference data (*51*) presented are representative of duplicate injections acquired from three independent trials. To predict overall equilibrium dissociation constants (K_D), steady-state binding responses (R_{eq}) were averaged near the end of the association phase, plotted as a function of VirB concentration (C), and then subjected to nonlinear regression analysis ("steady-state affinity" model, BIAevaluation version 4.1).

To assess complex formation, multicomponent analyses were performed in which fixed concentrations of VirB8, VirB9, and VirB10 (5 μM each) were passed over immobilized VirB8 at 10 μL/min using the "QUICKINJECT" mode (5 min association). After each sequential addition, the amount of VirB protein bound in a stable fashion was verified using two 30 s pulses of NaCl (0.5 M in HBS-EP) that removed transiently bound proteins. At the end of each multicomponent series, the immobilized VirB8 surface was regenerated at 50 μL/min using two 30 s pulses of solution III [Pierce Gentle Elution containing 0.1% (v/v) Empigen] and solution IV [HBS-EP containing 1 M NaCl, 50 mM EDTA, 10 mM NaOH, 0.1% (v/v) Tween 20, and 0.1% (v/v) Empigen], followed by "EXTRACLEAN" and "RINSE" procedures. Double-reference data (*51*) are representative of duplicate injections acquired from three independent trials.

Bacterial Two-Hybrid Assay. To test for VirB8, VirB9, and VirB10 interactions in vivo, the BTH system assay based on reconstitution of the AC active site was used (*52*, *53*). The genes encoding full-length VirB8, VirB8^{M102R}, and VirB10 were fused to the T18 and T25 fragments (encoding the catalytic domain of *Bordetella pertussis* AC) and bicistronic constructs coexpressing VirB9 and VirB10 were tested (*48*). Briefly, *E. coli* strain BTH101 was cotransformed with vectors expressing recombinant T25 and T18 fusions to VirB proteins and T25 and T18 domains alone as negative controls and cultivated in liquid LB medium with kanamycin (50 μg/mL), carbenicillin (100 μg/mL), and 1 mM IPTG for 16 h at 26 °C. The interactions were detected by determining the VirB interaction-mediated functional complementation of the two CyaA fragments that led to the production of cAMP, which triggered the β-galactosidase production in the BTH101 strain, and were quantified using ONPG as a substrate (*54*). The levels of VirB proteins expressed

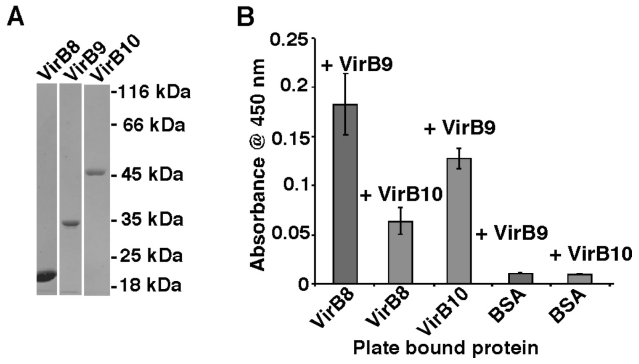

FIGURE 1: Qualitative analysis of VirB protein interactions using an antibody-based ELISA. (A) Representative SDS−PAGE (10% polyacrylamide) of soluble, periplasmic forms of strepIIVirB8, strepIIVirB9, and strepIIVirB10 purified to apparent homogeneity, like that for VirB8^{M102R} (not shown). (B) ELISA results depicting the binding of 50 pmol of VirB proteins (VirB9 or VirB10) to immobilized partners (VirB8, VirB10, or BSA), as detected using VirB protein-specific antisera, followed by secondary HRP-conjugated goat anti-rabbit IgG. Color development was measured after addition of the chromogenic solution containing HRP substrate, followed by addition of sulfuric acid to stop the reaction and measurement of the absorbance at 450 nm. The results from three independent experiments are shown, and bars represent the standard deviation.

in the BTH101 strain were assessed by electrophoresis of cell lysates on 10% SDS−PAGE standardized according to OD_{600}, followed by Western blotting using specific VirB antisera.

RESULTS

Qualitative Analysis of Interactions among VirB8, VirB9, and VirB10. To initiate the in vitro analysis of interactions among VirB8, VirB9, and VirB10, the periplasmic portions of the *B. suis* proteins, known to comprise the main functional domains, were overproduced and purified. We used strep-tactin affinity chromatography to isolate the three VirB proteins from *E. coli* lysates, followed by additional size exclusion (VirB8 and VirB8^{M102R}) or ion exchange (VirB9 and VirB10) chromatography. SDS−PAGE analysis (Figure 1A) demonstrated that all of the VirB preparations were purified to homogeneity (> 95%) and migrated at the anticipated molecular weights.

The purified strepII-tagged periplasmic domains of VirB proteins and BSA (negative control) were then coated to wells of NUNC microtiter plates to test for the binding of VirB8, VirB9, and VirB10 using ELISA-based detection. We observed binding of VirB9 and VirB10 to immobilized VirB8 and of VirB9 to immobilized VirB10 (Figure 1B), with little or no nonspecific binding of the VirB proteins to immobilized BSA under identical conditions. Because of the cross-reactivity of the VirB8 antiserum toward VirB9 and VirB10, we could not conduct reciprocal experiments with VirB8 binding to immobilized VirB9 and VirB10. Our ELISA results are consistent with interactions previously reported in the case of the homologous T4SS proteins from *A. tumefaciens* (*22*, *24*, *41*, *46*).

Conformational Changes upon Formation of the VirB8−VirB9−VirB10 Complex. Next, to assess the formation of VirB protein complexes, CD spectroscopy measurements of strepII-tagged periplasmic domains of VirB8, VirB9, and VirB10 were performed, measuring individual proteins and combinations. In comparison to the scans of individual proteins (Figure 2A−C), combining VirB8 and VirB9 led to a decrease in the ellipticity of the spectrum as compared to the calculated addition of the VirB8 and VirB9 spectra (data not shown), suggesting that there is a conformational change upon interaction. In contrast, combining VirB8−VirB10 and VirB9−VirB10 complexes led to an increase in ellipticity, and this also indicates conformational changes (data not shown). These observations suggest that structural changes occur when VirB8, VirB9, and VirB10 interact in a pairwise fashion. When all three proteins were mixed and a wavelength scan was performed, we noticed a large increase in ellipticity, which is notably different from the theoretical sum of the spectra of the three individual proteins (Figure 2D). These findings indicate that upon interaction, conformational changes occur. It is difficult to assess the secondary structure content from the CD scans; therefore, programs from CDpro collected were used to predict the secondary structure purely from CD scans, and programs from CDpro were used to predict the secondary structures of VirB8, VirB9, and VirB10, as well as that of the VirB8−VirB9−VirB10 complex. VirB8 was predicted to have a slightly higher percentage of β-strands (29.8%) than helices (22.2%) (Table 1), which is consistent with the X-ray structure (*55*, *56*). Most of VirB9 is predicted to be unordered (43.3%), and VirB10 is predicted to contain 41.3% β-strands (Table 1), which is consistent with the X-ray structure of the VirB10 homologue from *Helicobacter pylori* (ComB10) (*27*, *55*). Interestingly, the VirB8−VirB9−VirB10 complex is predicted to contain a higher α-helix content (49.9%), suggesting that upon complex formation, there is a large increase in the overall α-helix content indicating that conformational changes occur (Table 1).

Subsequently, we used scanning CD measurements of the thermal stability of the VirB proteins individually and in combinations to assess whether complex formation has an impact on their stability. This approach is commonly used to analyze protein complexes of unknown structure (*57*−*59*). The unfolding of VirB helical content was monitored at 222 nm as in previous work (*57*−*59*). Our analysis showed that VirB8 unfolds in a cooperative manner (Figure 3A). In contrast, VirB9's ellipticity increased beginning at 35 °C and the apparent α-helical content continued to increase with temperature. Finally, VirB10 unfolded in a noncooperative manner with an increase in temperature, and apparently, a small amount of helices was lost (Figure 3A). Next, proteins were analyzed in pairwise combinations to determine whether there are conformational changes upon interaction. The analysis of the VirB9−VirB10 complex did not yield interpretable results, and therefore, it was omitted from the analysis (data not shown). In the case of VirB8−VirB9 (Figure 3B), VirB8−VirB10 (Figure 3C), and VirB8−VirB9−VirB10 (Figure 3D) complexes, however, we observed clear transitions in their thermal denaturation curves. Therefore, the thermal denaturation studies indicate that upon interaction, conformational changes occur and were stabilized.

Quantitative Analysis of Interactions among VirB8, VirB9, and VirB10. To quantitatively characterize the interactions, we then analyzed the VirB protein interactions using label-free, real-time SPR. In a typical experiment, one protein is immobilized to the sensor chip surface and the binding partner(s) is then passed over the top in solution. Association and dissociation events are monitored by changes in molecular mass accumulation at the solid−liquid interface, commonly plotted as binding response (resonance units, RU) as a function of time (*60*). For our analyses, purified strepII-tagged periplasmic domains of VirB8, VirB9, and VirB10 were immobilized to the sensor chips via amine group coupling. Dose-dependent binding of VirB8 to immobilized VirB8 was detected, and this interaction was characterized by rapid association

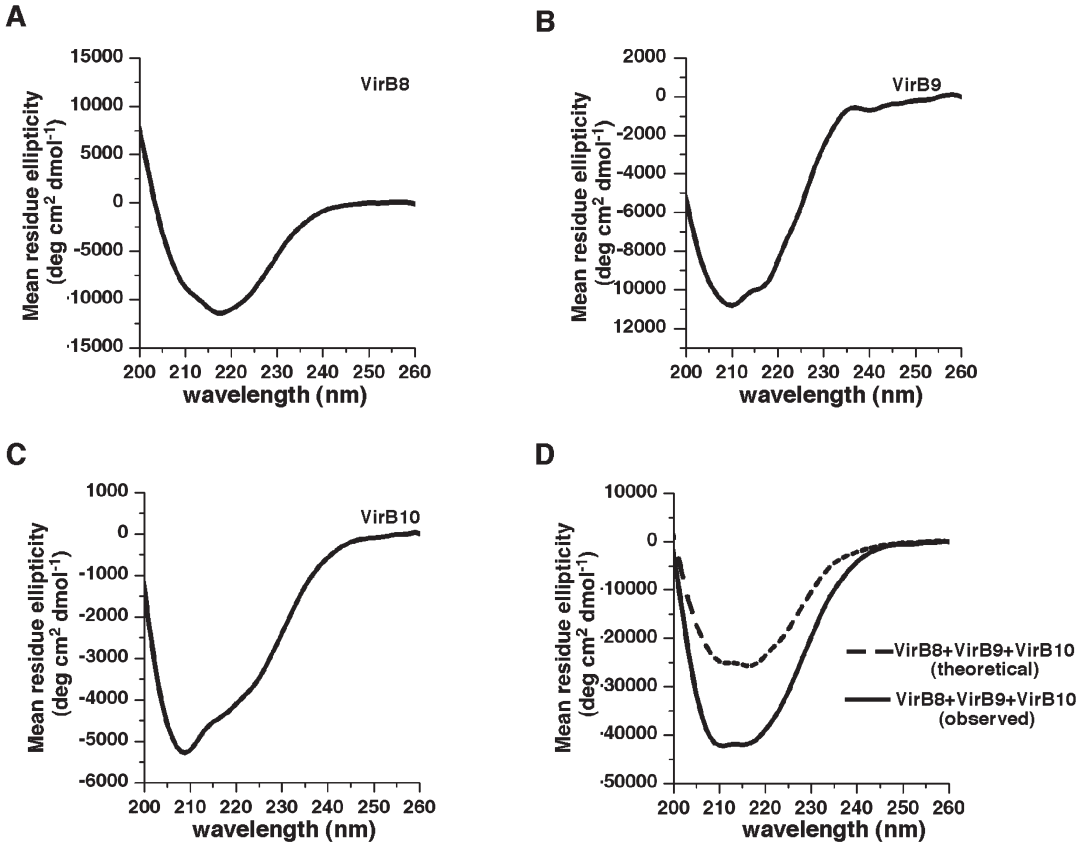

FIGURE 2: Analysis of interactions between VirB proteins using far-UV circular dichroism. Characterization of the structures of purified periplasmic domains of VirB8, VirB9, and VirB10 alone and in mixtures by CD spectroscopy. Spectra for 1250 pmol of VirB8 (A), VirB9 (B), and VirB10 (C) were acquired alone and in combinations at 25 °C. (D) The solid black line represents the result obtained after analysis of an equimolar mixture of VirB8, VirB9, and VirB10, whereas the dashed line represents the theoretical result representing the addition of the spectra of the three individual proteins.

Table 1: Predicted Secondary Structure of VirB8, VirB9, VirB10, and the VirB8−VirB9−VirB10 Complex from CD Scans Were Calculated Using SELCON and CONTINILL from CDpro

	% helix	% β-strand	% turn	% unordered
VirB8	22.2	29.8	19.8	28.2
VirB9	11.9	18.7	27.7	43.3
VirB10	5.8	41.3	18.7	29.4
VirB8−VirB9−VirB10	49.9	1.2	16.8	32.0

and rapid dissociation kinetics (Figure 4A). The micromolar VirB8−VirB8 affinity predicted by SPR ($K_D = 26 \pm 5$ μM) correlated well with our VirB8 self-association analysis (K_D=116 μM) previously quantified using AUC (*41*). While VirB8 binding to immobilized VirB9 and VirB10 surfaces yielded weak signal responses (Figure 4A), reciprocal titrations of VirB9 and VirB10 binding to immobilized VirB8 (Figure 4B,C) showed midnanomolar affinities ($K_D = 418 \pm 63$ and 218 ± 20 nM, respectively). Similarly, VirB9 and VirB10 binding to immobilized VirB9 ($K_D = 374 \pm 63$ and 216 ± 32 nM, respectively) and to immobilized VirB10 ($K_D = 443 \pm 59$ and 236 ± 38 nM, respectively) exhibited similar midnanomolar binding affinities (Figure 4B,C). Regardless of the immobilized VirB surface, the micromolar affinity seen in the case of the VirB8−VirB8 interaction [rapid-on and rapid-off kinetics (Figure 4A)] was distinctly different from the nanomolar affinity observed with VirB9 [fast-on and fast-off kinetics (Figure 4B)] and VirB10 [fast-on and slow-off kinetics (Figure 4C and Table 2)]. VirB10 had the overall highest affinity for its interaction partners followed by VirB9 and VirB8. These results demonstrate that the three VirB proteins have distinct binding properties (i.e., kinetics and affinities) that may be required for their biological functions. There was little or no nonspecific binding of BSA to the immobilized SPR surfaces, indicating that the VirB proteins interact only with specific binding partners (data not shown).

To further validate the specificity of our SPR results, we also characterized the binding of a VirB8 variant (M102R) previously shown to exhibit a reduced level of dimerization by analytical gel filtration and AUC (*41*, *48*). VirB8 and VirB8^{M102R} were immobilized and then titrated over a higher concentration series (up to 50 μM) as interactions were expected to be weaker. Wild-type VirB8 interacted strongly with itself, yielding a low micromolar K_D [23 ± 3 μM (Figure 5A)] that correlated well with the earlier titration series [$K_D = 26 \pm 5$ μM (Figure 4A)]. When VirB8 was titrated over VirB8^{M102R} [$K_D > 1$ mM (Figure 5B)] or VirB8^{M102R} was titrated over itself [$K_D > 1$ mM (Figure 5C)], very weak binding responses were observed compared to the wild-type VirB8−VirB8 interaction. These observations are consistent with the previous finding that VirB8^{M102R} is a dimer site variant and here validates the specificity of the binding interactions tested by SPR.

Formation of a Ternary Complex among VirB8, VirB9, and VirB10. We next performed multicomponent SPR analyses to test whether VirB8, VirB9, and VirB10 assemble into a ternary complex as predicted by current models of T4SS assembly. All three VirB proteins were injected into variable sequences over the immobilized VirB8 surface. For each series of injections, with intermittent salt washes to remove loosely bound protein, successive increases in the binding responses demonstrated that stable complexes formed (Figure 6). When VirB8 was passed over immobilized VirB8 followed by VirB9 and VirB10 (Figure 6A),

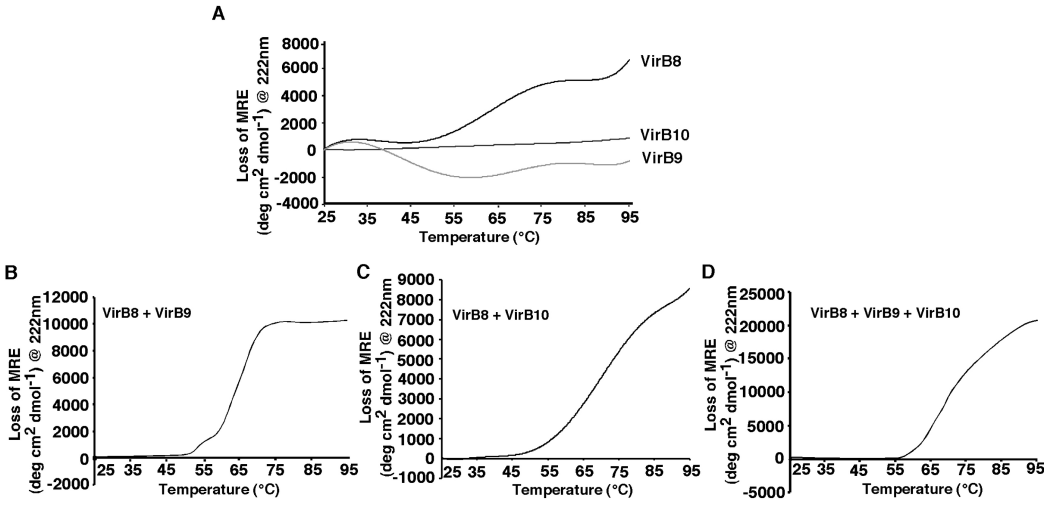

FIGURE 3: Stability of VirB proteins and complexes assessed by thermal denaturation and CD spectroscopy. (A) Analysis of the change in mean residue ellipticity (MRE) at 222 nm of VirB8, VirB9, and VirB10 as a function of temperature (25−95 °C). (B) Change in MRE at 222 nm of an equimolar mixture (1250 pmol) of VirB8 and VirB9 as a function of temperature. (C) Analysis of an equimolar mixture of VirB8 and VirB10. (D) Analysis of an equimolar mixture of VirB8, VirB9, and VirB10.

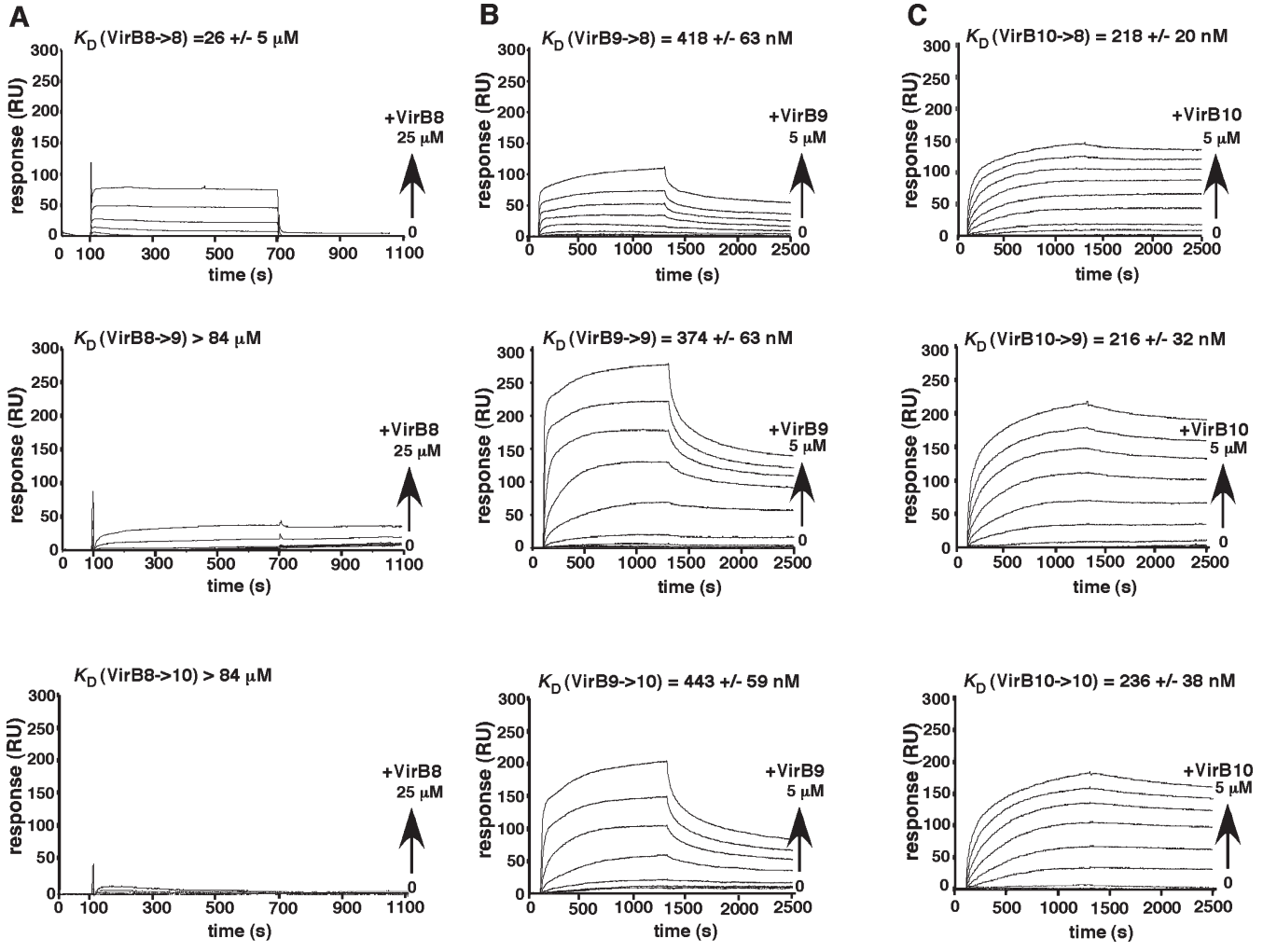

FIGURE 4: Quantitative analysis of VirB protein interactions using label-free, real-time SPR. Purified periplasmic VirB domains were amine coupled to CM4 sensor chips to final surface densities of 900 RU each. (A) VirB8 was passed over VirB8-, VirB9-, and VirB10-immobilized surfaces. (B) VirB9 was passed over VirB8-, VirB9-, and VirB10-immobilized surfaces. (C) VirB10 was passed over VirB8-, VirB9-, and VirB10-immobilized surfaces. Each VirB protein was titrated using a 2-fold dilution series, and the binding was monitored as a function of RU over time (seconds): VirB8, 0−25 μM, 10 min association and 10 min dissociation; VirB9, 0−5 μM, 20 min association and 20 min dissociation; VirB10, 0−5 μM, 20 min association and 20 min dissociation. Apparent equilibrium dissociation constants (K_D) were determined by plotting steady-state binding responses (R_{eq}) as a function of VirB concentration (C); resultant binding isotherms were fitted to a steady-state affinity model using BIAevaluation version 4.1. The results represent the average of three experiments ± the standard error.

the overall magnitude of complex formation (assessed by the final level of response, i.e., ~120 RU) was similar to the that from the experiment in which VirB9 was firstpassed over a VirB8-immobilized surface followed by VirB8 and VirB10 (Figure 6B). Similarly, when VirB10 was passed over immobilized VirB8 followed by VirB9 and VirB8 (Figure 6C), the final magnitude of complex formation was unaltered; an additional experiment in which VirB8 was passed over immobilized VirB8 followed by VirB10 and VirB9 was also unaltered (data not shown). Thus, ternary complexes formed in a manner independent of the order of injection over a VirB8-immobilized surface, suggesting that VirB8, VirB9, and VirB10 interact through distinct binding sites. Similar outcomes were observed using immobilized VirB9 and VirB10 surfaces (data not shown), further demonstrating that ternary complexes formed in a manner independent of the order of injection. The association and dissociation rates were independent of the order of VirB protein addition and were similar to the rates observed upon formation of each respective binary complex (Figure 4). Overall, these data provide the first direct evidence that VirB8, VirB9, and VirB10 can form a ternary complex in vitro.

A Bacterial Two-Hybrid Assay Detects Dynamic Associations among VirB8, VirB9, and VirB10. To complement the in vitro analyses with a more physiologically relevant assay, we applied the BTH system that is based on the reconstitution of the enzymatic activity of AC by interacting proteins fused to its two domains. Full-length versions of VirB8 and VirB10 were expressed in *E. coli* as fusions to the cytoplasmic T18 and T25 domains of AC, and their interaction was shown to restore cAMP production and ultimately β-galactosidase activity as readout (*53*). We here tested more complex interactions among core complex components. To this end, we generated bicistronic constructs that permitted the simultaneous expression of proteins not fused to the AC domains (Figure 7A). When VirB9 was coexpressed in the periplasm with VirB8 fused to the AC domains, we observed strongly increased β-galactosidase activity (3.8-fold), indicating that VirB9 stimulated VirB8 self-association (Figure 7B). In contrast, the coexpression of VirB10 did not affect VirB8 self-association. The coexpression of VirB9 weakened the VirB8−VirB10 interaction to 15% of the control, and similarly, expression of VirB9 weakened the VirB10−VirB10 interaction to 38%. In contrast, expression of VirB10 further strengthened VirB10 self-association 1.5-fold (Figure 7B). These results show that VirB9 modulates the homomeric and heteromeric interactions between VirB8 and VirB10, which suggest a previously unassigned role for this protein in T4SS assembly. The reduced level of dimerization of the purified VirB8^{M102R} variant was shown by AUC and here by SPR. As expected, fusions of the VirB8^{M102R} variant with AC domains resulted in reduced β-galactosidase activity, indicating a reduced level of dimerization (Figure 7B). However, when this variant was tested in a bicistronic construct coexpressed with VirB9, an increase in β-galactosidase activity was observed, suggesting that binding to VirB9 is not negatively impacted by the change. Similarly, the BTH assay showed that the VirB8^{M102R} variant was not affected in its interaction with VirB10 (Figure 7B), suggesting that this residue and dimerization are not important for VirB9 as well as for VirB10 binding.

To assess the levels of VirB8−VirB10 fusion proteins in the BTH101 strain, the cell lysates were separated by SDS−PAGE, followed by Western blotting using VirB-specific antisera. It was interesting to note that levels of VirB8 protein did not change when the β-galactosidase activity increased in the presence of VirB9 (Figure 7C). However, VirB8 was not detected in cells that served as a negative control when the T18 catalytic fragment was expressed with T25-fused VirB8. In addition, the VirB8 protein level was lower when VirB9 was coexpressed in the presence of T25-fused VirB8 and T18-fused VirB10, and in this case, the β-galactosidase activity was reduced (Figure 7C). A similar observation was made when VirB9 was expressed in the presence of T25VirB10 and T18VirB10 (Figure 7C). In addition, the protein level was also reduced when the VirB8 dimer site variant (VirB8^{M102R}) was tested using the BTH system. Therefore, the levels of the hybrid proteins were reduced as a consequence of weakened interactions, which may leave them more susceptible to degradation by periplasmic proteases. Overall, these results show that the BTH system is well-suited to the study of the dynamic interactions between VirB proteins in a simplified system for T4SS assembly.

Table 2: Apparent Equilibrium Dissociation Constants Determined for VirB Protein Interactions

equilibrium SPR analysis	K_D
VirB8 → VirB8	26 ± 5 μM
VirB8 → VirB9	> 84 μM
VirB8 → VirB10	> 84 μM
VirB9 → VirB8	418 ± 63 nM
VirB9 → VirB9	374 ± 63 nM
VirB9 → VirB10	443 ± 59 nM
VirB10 → VirB8	218 ± 20 nM
VirB10 → VirB9	216 ± 32 nM
VirB10 → VirB10	236 ± 38 nM
VirB8^{M102R} → VirB8	> 1 mM
VirB8^{M102R} → VirB8^{M102R}	> 1 mM

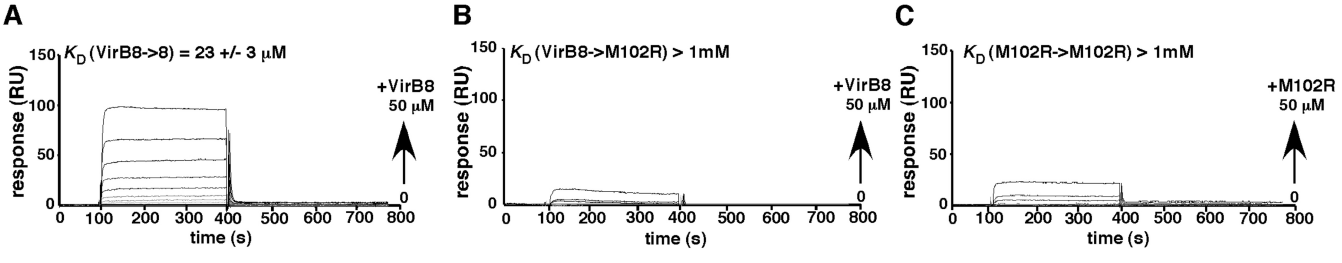

FIGURE 5: Quantitative analysis of VirB8^{M102R} self-association using label-free, real-time SPR. Purified periplasmic VirB domains were amine coupled to CM4 sensor chips to final surface densities of 900 RU each. (A) VirB8 was passed over a VirB8-immobilized surface. (B) VirB8^{M102R} was passed over a VirB8-immobilized surface. (C) VirB8^{M102R} was passed over a VirB8^{M102R}-immobilized surface. VirB8 and VirB8^{M102R} proteins were titrated using a 2-fold dilution series, and the binding was monitored as a function of RU over time (seconds): 0−50 μM, 10 min association and 10 min dissociation. Apparent equilibrium dissociation constants (K_D) were determined by plotting steady-state binding responses (R_{eq}) as a function of VirB concentration (C); resultant binding isotherms were fitted to a steady-state affinity model using BIAevaluation version 4.1. The results represent the average of three experiments ± the standard error.

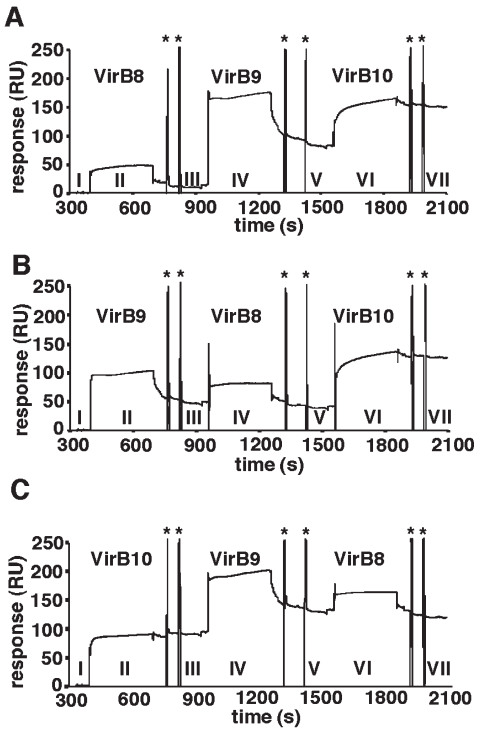

FIGURE 6: Observation of formation of the ternary complex of VirB proteins using multicomponent SPR. Purified periplasmic domains of VirB8, VirB9, or VirB10 (5 μM each, different injection orders) were passed over an ~900 RU, amine-coupled VirB8 surface: (I) starting baseline, (II) injection of the first protein, (III) stable complex after two 0.5 M NaCl pulses to elute loosely bound proteins indicated with asterisks, (IV) injection of the second protein, (V) stable complex after two 0.5 M NaCl pulses to elute loosely bound proteins indicated by asterisks, (VI) injection of the third protein, and (VII) stable complex after 0.5 M NaCl pulses indicated by asterisks to elute loosely bound proteins and assess the final stable complex. (A) Binding responses beginning with VirB8 injection followed by VirB9 and VirB10 injections. (B) Binding responses beginning with VirB9 injection followed by VirB8 and VirB10 injections. (C) Binding responses beginning with VirB10 injection followed by VirB9 and VirB8 injections.

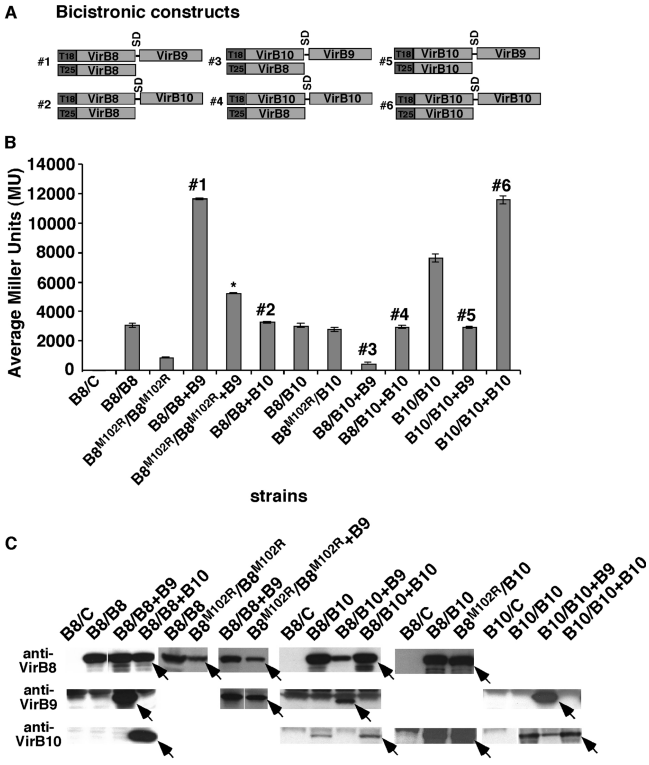

FIGURE 7: In vivo analysis of VirB protein interactions using the bacterial two-hybrid assay. As a simplified model system for studying T4SS core complex interactions, VirB8, VirB8^{M102R}, and VirB10 were fused to the T18 and T25 domains of adenylate cyclase (AC), and we determined the impacts of coexpression of a third protein produced in the periplasm. (A) Schematic view of the bicistronic constructs generated to test the effects of a third VirB protein on pairwise interactions. T18 and T25 denote the two domains of AC and SD, the Shine Dalgarno sequence. (B) Quantification of VirB interactions in *E. coli* strain BTH101 carrying plasmids encoding T18 and T25 fusions to VirB8−VirB10 and bicistronic constructs. Error bars represent the standard deviation of three independent measurements. C represents the negative control plasmid-expressing T18 fragment not fused to a protein. The numbers above the bars correspond to the strains carrying the constructs represented schematically in panel A. The asterisk denotes the bicistronic construct in which variant VirB8^{M102R} is coexpressed with VirB9. (C) Western blot detection of VirB8, VirB8^{M102R}, VirB9, and VirB10 protein levels using specific VirB antisera from *E. coli* strain BTH101 carrying the plasmids encoding T18 and T25 fusions to VirB8−VirB10 and bicistronic constructs as analyzed in panel B. Arrows indicate the VirB proteins identified with the VirB-specific antisera.

DISCUSSION

T4SS function depends on the formation of a complex between VirB proteins. To improve our understanding of how this machinery assembles, we characterized the interactions among the conserved core complex components VirB8, VirB9, and VirB10. The detection of VirB8−VirB9, VirB8−VirB10, and VirB9−VirB10 interactions by an ELISA indicated that the *B. suis* proteins purified were functionally active and corroborated interaction data previously acquired using *A. tumefaciens* homologues.

To study the *B. suis* proteins in greater detail, we used CD spectroscopy to assess whether VirB interactions trigger conformational changes. Both far-UV wavelength scans and thermal denaturation were previously utilized to analyze the structural changes that occur when proteins form complexes in solution (*58*, *59*). This approach demonstrated complex formation of three proteins (PscE, PscF, and PscG) involved in needle biogenesis of a type III secretion system (*57*). Using CD scans, we demonstrated that structural changes occur when VirB8, VirB9, and VirB10 are mixed, and this is indicative of dynamic interactions (Figure 2). Thermal scans showed that VirB8 unfolds in a cooperative fashion, whereas VirB9 and VirB10 alone are thermodynamically stable, as they did not exhibit a clear T_m. This case is comparable to the PscF needlelike protein that exhibited a curve in thermal scans similar to that of VirB10. The authors of this study proposed that PscF is present in a lower energetic state and that it aggregated into a structure that could not be changed by heat (*57*). However, in the presence of the interaction partners (PscE and PscG), PscF was recruited into complexes that were more stable, indicated by a thermal denaturation curve of the PscE, PscG, and PscF mixture that had a T_m higher than those of PscE and PscG. Similarly, we propose that VirB8 forms stable binary interactions with VirB9 and VirB10. This further supports the hypothesis that the interaction of VirB8 with VirB9 and VirB10 may lead to the recruitment of the proteins into a polar T4SS assembly as proposed previously (*45*). The action of VirB8 may prevent a biologically nonproductive aggregation of VirB9 and VirB10.

To characterize the VirB8, VirB9, and VirB10 interactions in a quantitative fashion, we then utilized SPR. Signal responses for

VirB8 flowing over immobilized VirB9 and VirB10 were weak, but VirB9 and VirB10 injected over immobilized VirB8 yielded dose-dependent, saturable binding responses. This effect may be due to the masking of key binding residues for VirB8 by the amine coupling of VirB9 and VirB10 to the sensor chip. In agreement with previous AUC data, the periplasmic VirB8−VirB8 interaction exhibited a micromolar binding affinity constant. The relatively weak VirB8 self-association and the fast-on and fast-off kinetics may be important for rapid dimer formation and dissociation. Physiologically, this suggests that VirB8 may rapidly mediate other VirB protein interactions required for T4SS assembly. In support of this hypothesis, VirB8 was postulated to be a nucleation factor for T4SS assembly (*45*) and shown to interact with many other VirB proteins (*22*−*24*, *41*, *61*). Furthermore, rapid association and dissociation of the VirB8 dimers may be necessary for its interaction with other VirB proteins as a T4SS assembly factor. Our work suggests that such an interaction occurs with VirB5 to facilitate pilus assembly (ref *23* and unpublished data of Sivanesan et al., 2010). Interestingly, the other periplasmic VirB interaction pairs exhibited midnanomolar binding affinities, suggesting that they may be primarily structural components. The higher-affinity interactions of VirB9 and VirB10 and the fast-on and slow-off kinetics of VirB10 interactions are in accord with the requirement of stabilizing the core complex once assembled. Next, as in the FhuA−TonB−FhuD system (*62*), we adopted a multicomponent style of SPR analysis and demonstrated that VirB8, VirB9, and VirB10 form a ternary complex. The multicomponent SPR analysis builds upon recent cryo-EM and crystallographic studies in which VirB8 was not detected or required for the formation of the VirB7−VirB9−VirB10 T4SS core complex (*18*, *27*). All the available data indicate that VirB8 is required for T4SS assembly and correct subcellular localization under natural conditions, but under conditions of artificial overexpression of the components for structural studies, it is apparently not essential. This is consistent with our finding that the affinity of VirB8 is relatively weak, suggesting that it acts in a transient fashion as an assembly factor that may be only loosely associated with the final T4SS core complex in vivo. VirB8 was cross-linked to the translocated T-DNA substrate in *Agrobacterium*, but this merely indicates its localization and does not necessarily imply that it is an active component of the translocation machinery; the available data are consistent with a primary role as a protein assembly factor.

As the final approach to examining the dynamic nature of interactions among *B. suis* VirB8, VirB9, and VirB10, we utilized the BTH system in vivo. This assay permits the analysis of full-length proteins in their natural environment, the periplasm of a Gram-negative cell. This experimental approach was previously applied to characterize the VirB8−VirB10 interaction (*53*, *63*), VirB8 self-association (*53*), and VirB8 dimer variants (*48*). The use of bicistronic constructs demonstrated that VirB9 stabilizes VirB8 dimers but that VirB10 had no impact on the dimerization of VirB8. This was further supported by the VirB8^{M102R} dimer variant, which was stabilized by VirB9, and this variant was not affected by interaction with VirB10. Therefore, it is reasonable to hypothesize that VirB8 dimers interact with VirB9 and with VirB10 dimers to target these proteins to poles of the bacterial cells. In addition, VirB9 stabilized VirB8 dimers but dissociated VirB8−VirB10 and VirB10−VirB10 dimers, which suggests an important regulatory function for VirB9 in T4SS core complex assembly. It is possible that the affinity between VirB9 and VirB10 in vivo is stronger than that between VirB8 and VirB10 or between VirB8 and VirB9, leading to dissociation of VirB8−VirB10 and VirB8−VirB9 heterodimers. The SPR results, however, did not show large differences in the affinities of VirB8−VirB9, VirB8−VirB10, VirB9−VirB10, and VirB10−VirB10 complexes, but VirB10 was generally the strongest binding partner. It is possible that the periplasmic-only domains of VirB8 and VirB10 utilized in the in vitro SPR experiments do not completely mimic the full-length proteins in the in vivo BTH experiments that may adopt alternative conformations in the periplasm. Future studies are also needed to examine whether the transmembrane domains may influence the overall binding affinities.

Several lines of evidence support our proposed model of T4SS core complex assembly. First, VirB8 self-associates as identified in this study and as previously reported, and it exists in a monomer−dimer equilibrium (*41*). VirB9 localizes in the periplasm and interacts with VirB7 (*28*, *35*, *64*), and VirB9 and VirB10 form homomultimers. This step is followed by interaction of the VirB8 dimer with VirB9 and VirB10 to mediate their colocalization (*45*) (Figure 7B). VirB9 stabilizes VirB8 self-association, and nucleation by VirB8 facilitates the VirB9−VirB10 interaction and presumably the formation of the functional complex observed by cryo-EM and crystallography (*18*, *27*). This model is further supported by additional results of the BTH assay, namely the fact that VirB10 stimulates VirB10−VirB10 interaction, a process that could represent unproductive aggregation. VirB9 weakened this interaction as well as the VirB8−VirB10 interaction, and this may explain why VirB8 was not cocrystallized with the VirB7−VirB9−VirB10 complex (*18*, *27*). This model is also supported by the results of CD spectroscopy experiments that demonstrated that mixtures of VirB proteins (VirB8−VirB9, VirB8−VirB10, and VirB8−VirB9−VirB10) were more stable than the individual proteins. Moreover, accumulation of VirB9 was previously suggested to cause conformational changes in VirB10 and may thereby interfere with VirB10 self-association (*38*, *65*, *66*). Furthermore, an in-frame deletion of the *virB9* gene reduced the stability of VirB4, VirB8, VirB10, and VirB11 in *A. tumefaciens* cells, indicating a role of VirB9 in stabilization of VirB8 and VirB10 (*40*). We propose that VirB8 acts as an assembly factor to bring VirB9 and VirB10 to the poles of the bacteria. As the next step, VirB9, an intermediate in the complex as shown by its fast-on and fast-off kinetics, interacts with VirB10, inducing conformational changes that reduce the level of unproductive aggregation and dissociate VirB10 from VirB8. VirB10 displays fast-on and slow-off kinetics and the highest binding affinities, which suggests that the interaction of VirB10 with VirB9 occurs later in the sequence of interactions. In contrast, interactions of VirB8 (fast-on and fast-off) with VirB9 and VirB10 suggest a transient role as a scaffolding protein in T4SS assembly that may be only loosely attached to the final complex (*18*, *27*).

In summary, the results presented here not only validate previously described VirB8, VirB9, and VirB10 interactions but also provide novel quantitative (i.e., real-time binding kinetics and affinity), structural (i.e., ternary complex formation), in vivo (i.e., BTH assay), and dynamic (i.e., proposed assembly model) insights into T4SS core complex assembly. Future work will identify the VirB protein domains and residues that are specifically required for complex formation. Importantly, following the approaches developed here, other VirB proteins could be added to determine their influence on formation of the VirB8−VirB9−VirB10 complex. For instance, the effects of VirB7 on

VirB8−VirB9−VirB10 interactions will be tested in the future. VirB7 stabilizes VirB9 and interacts via a covalent bond in *A. tumefaciens* T4SS (*30*, *31*, *35*), and its interaction with VirB9 may influence the interaction of VirB9 with VirB8 and VirB10. The influence of the cytoplasmic and transmembrane domains of VirB8 and VirB10 proteins on binding affinities should also be assessed using purified full-length proteins. Overall, this study builds upon previous literature and proposes a defined sequence of binding interactions that ultimately leads to the assembly of the core T4SS complex. The proposed model will help to define potential targets for the development of new antimicrobials.

ACKNOWLEDGMENT

Thanks to Dr. Raquel Epand for help with CD spectroscopy experiments. Thanks to Chan Gao, Michelle Melone, Dr. Athanasios Paschos, Dr. George Sorger, and Dr. Douglas Davidson for critical discussion.

SUPPORTING INFORMATION AVAILABLE

Description of plasmids and strains (Table 1) and a list of oligonucleotides used for construction of plasmids (Table 2). This material is available free of charge via the Internet at http://pubs.acs.org.

REFERENCES

1. Llosa, M., and O'Callaghan, D. (2004) Euroconference on the Biology of Type IV Secretion Processes: Bacterial gates into the outer world. *Mol. Microbiol. 53*, 1–8.
2. Christie, P. J. (2004) Type IV secretion: The *Agrobacterium* VirB/D4 and related conjugation systems. *Biochim. Biophys. Acta 1694*, 219–234.
3. Cascales, E., and Christie, P. J. (2003) The versatile bacterial type IV secretion systems. *Nat. Rev. Microbiol. 1*, 137–149.
4. Baron, C., O'Callaghan, D., and Lanka, E. (2002) Bacterial secrets of secretion: EuroConference on the biology of type IV secretion processes. *Mol. Microbiol. 43*, 1359–1366.
5. Baron, C. (2005) From bioremediation to biowarfare: On the impact and mechanism of type IV secretion systems. *FEMS Microbiol. Lett. 253*, 163–170.
6. Baron, C., and Zambryski, P. C. (1996) Plant Transformation: A pilus in *Agrobacterium* T-DNA transfer. *Curr. Biol. 6*, 1567–1569.
7. O'Callaghan, D., Cazevieille, C., Allardet-Servent, A., Boschiroli, M. L., Bourg, G., Foulongne, V., Frutos, P., Kulakov, Y., and Ramuz, M. (1999) A homologue of the *Agrobacterium tumefaciens* VirB and *Bordetella pertussis* Ptl type IV secretion systems is essential for intracellular survival of *Brucella suis*. *Mol. Microbiol. 33*, 1210–1220.
8. de Jong, M. F., Sun, Y. H., den Hartigh, A. B., van Dijl, J. M., and Tsolis, R. M. (2008) Identification of VceA and VceC, two members of the VjbR regulon that are translocated into macrophages by the *Brucella* type IV secretion system. *Mol. Microbiol. 70*, 1378–1396.
9. Roux, C. M., Rolan, H. G., Santos, R. L., Beremand, P. D., Thomas, T. L., Adams, L. G., and Tsolis, R. M. (2007) *Brucella* requires a functional Type IV secretion system to elicit innate immune responses in mice. *Cell. Microbiol. 9*, 1851–1869.
10. O'Callaghan, D., Cazevieille, C., Allardet-Servent, A., Boschiroli, M. L., Bourg, G., Foulongne, V., Frutus, P., Kulakov, Y., and Ramuz, M. (1999) A homologue of the *Agrobacterium tumefaciens* VirB and *Bordetella pertussis* Ptl type IV secretion systems is essential for intracellular survival of *Brucella suis*. *Mol. Microbiol. 33*, 1210–1220.
11. Guo, M., Jin, S., Sun, D., Hew, C. L., and Pan, S. Q. (2007) Recruitment of conjugative DNA transfer substrate to *Agrobacterium* type IV secretion apparatus. *Proc. Natl. Acad. Sci. U.S.A. 104*, 20019–20024.
12. Atmakuri, K., Ding, Z., and Christie, P. J. (2003) VirE2, a type IV secretion substrate, interacts with the VirD4 transfer protein at cell poles of *Agrobacterium tumefaciens*. *Mol. Microbiol. 49*, 1699–1713.
13. den Hartigh, A. B., Sun, Y. H., Sondervan, D., Heuvelmans, N., Reinders, M. O., Ficht, T. A., and Tsolis, R. M. (2004) Differential requirements for VirB1 and VirB2 during *Brucella abortus* infection. *Infect. Immun. 72*, 5143–5149.
14. den Hartigh, A. B., Rolan, H. G., de Jong, M. F., and Tsolis, R. M. (2008) VirB3 to VirB6 and VirB8 to VirB11, but not VirB7, are essential for mediating persistence of *Brucella* in the reticuloendothelial system. *J. Bacteriol. 190*, 4427–4436.
15. Sun, Y. H., Garcia-Rolan, H., den Hartigh, A. B., Sondervan, D., and Tsolis, R. M. (2005) *Brucella abortus* VirB12 is expressed during infection, but it is not an essential component of the type IV secretion system. *Infect. Immun. 73*, 6048–6054.
16. Zahrl, D., Wagner, M., Bischof, K., Bayer, M., Zavecz, B., Beranek, A., Ruckenstuhl, C., Zarfel, G. E., and Koraimann, G. (2005) Peptidoglycan degradation by specialized lytic transglycosylases associated with type III and type IV secretion systems. *Microbiology 151*, 3455–3467.
17. Zupan, J., Hackworth, C. A., Aguilar, J., Ward, D., and Zambryski, P. (2007) VirB1* promotes T-pilus formation in the vir-Type IV secretion system of *Agrobacterium tumefaciens*. *J. Bacteriol. 189*, 6551–6563.
18. Fronzes, R., Schafer, E., Wang, L., Saibil, H. R., Orlova, E. V., and Waksman, G. (2009) Structure of a type IV secretion system core complex. *Science 323*, 266–268.
19. Christie, P. J., Atmakuri, K., Krishnamoorthy, V., Jakubowski, S., and Cascales, E. (2005) Biogenesis, Architecture, and Function of Bacterial Type IV Secretion Systems. *Annu. Rev. Microbiol. 59*, 415–485.
20. Carle, A., Höppner, C., Aly, K. A., Yuan, Q., den Dulk-Ras, A., Vergunst, A., O'Callaghan, D., and Baron, C. (2006) The *Brucella suis* type IV secretion system assembles in the cell envelope of the heterologous host *Agrobacterium tumefaciens* and increases IncQ plasmid pLS1 recipient competence. *Infect. Immun. 74*, 108–117.
21. Krall, L., Wiedemann, U., Unsin, G., Weiss, S., Domke, N., and Baron, C. (2002) Detergent extraction identifies different VirB protein subassemblies of the type IV secretion machinery in the membranes of *Agrobacterium tumefaciens*. *Proc. Natl. Acad. Sci. U.S.A. 99*, 11405–11410.
22. Ward, D., Draper, O., Zupan, J. R., and Zambryski, P. C. (2002) Peptide linkage mapping of the *A. tumefaciens vir*-encoded type IV secretion system reveals novel protein subassemblies. *Proc. Natl. Acad. Sci. U.S.A. 99*, 11493–11500.
23. Yuan, Q., Carle, A., Gao, C., Sivanesan, D., Aly, K., Höppner, C., Krall, L., Domke, N., and Baron, C. (2005) Identification of the VirB4-VirB8-VirB5-VirB2 pilus assembly sequence of type IV secretion systems. *J. Biol. Chem. 280*, 26349–26359.
24. Das, A., and Xie, Y.-H. (2000) The *Agrobacterium* T-DNA transport pore proteins VirB8, VirB9 and VirB10 interact with one another. *J. Bacteriol. 182*, 758–763.
25. Vetsch, M., Erilov, D., Moliere, N., Nishiyama, M., Ignatov, O., and Glockshuber, R. (2006) Mechanism of fibre assembly through the chaperone-usher pathway. *EMBO Rep. 7*, 734–738.
26. Vitagliano, L., Ruggiero, A., Pedone, C., and Berisio, R. (2007) A molecular dynamics study of pilus subunits: Insights into pilus biogenesis. *J. Mol. Biol. 367*, 935–941.
27. Chandran, V., Fronzes, R., Duquerroy, S., Cronin, N., Navaza, J., and Waksman, G. (2009) Structure of the outer membrane complex of a type IV secretion system. *Nature 29*, 29.
28. Das, A., Anderson, L. B., and Xie, Y.-H. (1997) Delineation of the interaction domains of *Agrobacterium tumefaciens* VirB7 and VirB9 by use of the yeast two-hybrid assay. *J. Bacteriol. 179*, 3404–3409.
29. Anderson, L. B., Vogel Hertzel, A., and Das, A. (1996) *Agrobacterium tumefaciens* VirB7 and VirB9 form a disulfide-linked protein complex. *Proc. Natl. Acad. Sci. U.S.A. 93*, 8889–8894.
30. Fernandez, D., Dang, T. A. T., Spudich, G. M., Zhou, X.-R., Berger, B. R., and Christie, P. J. (1996) The *Agrobacterium tumefaciens virB7* gene product, a proposed component of the T-complex transport apparatus, is a membrane-associated lipoprotein exposed at the periplasmic surface. *J. Bacteriol. 178*, 3156–3167.
31. Fernandez, D., Spudich, G. M., Zhou, X.-R., and Christie, P. J. (1996) The *Agrobacterium tumefaciens virB7* lipoprotein is required for stabilization of VirB proteins during assembly of the T-complex transport apparatus. *J. Bacteriol. 178*, 3168–3176.
32. Jakubowski, S. J., Krishnamoorthy, V., and Christie, P. J. (2003) *Agrobacterium tumefaciens* VirB6 protein participates in formation of VirB7 and VirB9 complexes required for type IV secretion. *J. Bacteriol. 185*, 2867–2878.
33. Das, A., and Xie, Y.-H. (1998) Construction of transposon Tn3*phoA*: Its application in defining the membrane topology of the *Agrobacterium tumefaciens* DNA transfer proteins. *Mol. Microbiol. 27*, 405–414.

34. Beijersbergen, A., Smith, S. J., and Hooykaas, P. J. J. (1994) Localization and topology of VirB proteins of *Agrobacterium tumefaciens*. *Plasmid 32*, 212–218.
35. Baron, C., Thorstenson, Y. R., and Zambryski, P. C. (1997) The lipoprotein VirB7 interacts with VirB9 in the membranes of *Agrobacterium tumefaciens*. *J. Bacteriol. 179*, 1211–1218.
36. Liu, Z., and Binns, A. N. (2003) Functional subsets of the VirB type IV transport complex proteins involved in the capacity of *Agrobacterium tumefaciens* to serve as a recipient in *virB*-mediated conjugal transfer of plasmid RSF1010. *J. Bacteriol. 185*, 3259–3269.
37. Kumar, R. B., Xie, Y.-H., and Das, A. (2000) Subcellular localization of the *Agrobacterium tumefaciens* T-DNA transport pore proteins: VirB8 is essential for assembly of the transport pore. *Mol. Microbiol. 36*, 608–617.
38. Beaupré, C. E., Bohne, J., Dale, E. M., and Binns, A. N. (1997) Interactions between VirB9 and VirB10 membrane proteins involved in movement of DNA from *Agrobacterium tumefaciens* into plant cells. *J. Bacteriol. 179*, 78–89.
39. Cascales, E., and Christie, P. J. (2004) *Agrobacterium* VirB10, an ATP energy sensor required for type IV secretion. *Proc. Natl. Acad. Sci. U. S.A. 101*, 17228–17233.
40. Berger, B. R., and Christie, P. J. (1994) Genetic complementation analysis of the *Agrobacterium tumefaciens virB* operon: *virB2* through *virB11* are essential virulence genes. *J. Bacteriol. 176*, 3646–3660.
41. Paschos, A., Patey, G., Sivanesan, D., Bayliss, R., Waksman, G., O'Callaghan, D., and Baron, C. (2006) Dimerization and interactions of *Brucella suis* VirB8 with VirB4 and VirB10 are required for its biological activity. *Proc. Natl. Acad. Sci. U.S.A. 103*, 7252–7257.
42. Ward, J. E., Dale, E. M., Nester, E. W., and Binns, A. N. (1990) Identification of a VirB10 protein aggregate in the inner membrane of *Agrobacterium tumefaciens*. *J. Bacteriol. 172*, 5200–5210.
43. Jakubowski, S. J., Cascales, E., Krishnamoorthy, V., and Christie, P. J. (2005) *Agrobacterium tumefaciens* VirB9, an outer-membrane-associated component of a type IV secretion system, regulates substrate selection and T-pilus biogenesis. *J. Bacteriol. 187*, 3486–3495.
44. Kumar, R. B., and Das, A. (2001) Functional analysis of the *Agrobacterium tumefaciens* T-DNA transport pore protein VirB8. *J. Bacteriol. 183*, 3636–3641.
45. Judd, P. K., Kumar, R. B., and Das, A. (2005) Spatial location and requirements for the assembly of the *Agrobacterium tumefaciens* type IV secretion apparatus. *Proc. Natl. Acad. Sci. U.S.A. 102*, 11498–11503.
46. Ding, Z., Zhao, Z., Jakubowski, S., Krishnamohan, A., Margolin, W., and Christie, P. J. (2002) A novel cytology-based, two-hybrid screen for bacteria applied to protein-protein interaction studies of a type IV secretion system. *J. Bacteriol. 184*, 5572–5582.
47. Maniatis, T. A., Fritsch, E. F., and Sambrook, J. (1982) Molecular Cloning: A Laboratory Manual, Cold Spring Harbor Laboratory Press, Plainview, NY.
48. Paschos, A., den Hartig, A., Coincon, M., Sivanesan, D., Sygusch, J., Tsolis, R. M., and Baron, C. (2010) An *in vivo* high-throughput screening approach targeting the type IV secretion system component VirB8 identified inhibitors of intracellular proliferation of *Brucella*. *PLoS Pathog*., submitted.
49. Taneva, S., Johnson, J. E., and Cornell, R. B. (2003) Lipid-Induced Conformational Switch in the Membrane Binding Domain of CTP: Phosphocholine Cytidyltransferase: A Circular Dichroism Study. *Biochemistry 42*, 11768–11776.
50. Sreerama, N., and Woody, R. W. (2000) Estimation of protein secondary structure from circular dichroism spectra: Comparison of CONTIN, SELCON, and CDSSTR methods with an expanded reference set. *Anal. Biochem. 287*, 252–260.
51. Myszka, D. G. (1999) Improving biosensor analysis. *J. Mol. Recognit. 12*, 279–284.
52. Karimova, G., Pidoux, J., Ullmann, A., and Ladant, D. (1998) A bacterial two-hybrid system based on a reconstituted signal transduction pathway. *Proc. Natl. Acad. Sci. U.S.A. 95*, 5752–5756.
53. Bourg, G., Sube, R., O'Callaghan, D., and Patey, G. (2009) Interactions between *Brucella suis* VirB8 and its homolog TraJ from the plasmid pSB102 underline the dynamic nature of type IV secretion systems. *J. Bacteriol. 191*, 2985–2992.
54. Cowie, A., Cheng, J., Sibley, C. D., Fong, Y., Zaheer, R., Patten, C. L., Morton, R. M., Golding, G. B., and Finan, T. M. (2006) An Integrated Approach to Functional Genomics: Construction of a Novel Reporter Gene Fusion Library for *Sinorhizobium meliloti*. *Appl. Environ. Microbiol. 72*, 7156–7167.
55. Terradot, L., Bayliss, R., Oomen, C., Leonard, G., Baron, C., and Waksman, G. (2005) Crystal Structures of the periplasmic domains of two core subunits of the bacterial type IV secretion system, VirB8 from *Brucella suis* and ComB10 from *Helicobacter pylori*. *Proc. Natl. Acad. Sci. U.S.A. 102*, 4596–4601.
56. Bailey, S., Ward, D., Middleton, R., Grossmann, J. G., and Zambryski, P. (2006) *Agrobacterium tumefaciens* VirB8 structure reveals potential protein-protein interactions sites. *Proc. Natl. Acad. Sci. U.S.A. 103*, 2582–2587.
57. Quinaud, M., Chabert, J., Faudry, E., Neumann, E., Lemaire, D., Pastor, A., Elsen, S., Dessen, A., and Attree, I. (2005) The PscE-PscF-PscG complex controls type III secretion needle biogenesis in *Pseudomonas aeruginosa*. *J. Biol. Chem. 280*, 36293–36300.
58. Nanao, M., Ricard-Blum, S., Di Guilmi, A. M., Lemaire, D., Lascoux, D., Chabert, J., Attree, I., and Dessen, A. (2003) Type III secretion proteins PcrV and PcrG from *Pseudomonas aeruginosa* form a 1:1 complex through high affinity interactions. *BMC Microbiol. 3*, 21.
59. Greenfield, N. J., and Fowler, V. M. (2002) Tropomyosin requires an intact N-terminal coiled coil to interact with tropomodulin. *Biophys. J. 82*, 2580–2591.
60. De Crescenzo, G., Boucher, C., Durocher, Y., and Jolicoeur, M. (2008) Kinetic characterization by surface plasmon resonance-based biosensors: Principle and emerging trends. *Cell. Mol. Bioeng. 1*, 204–215.
61. Höppner, C., Carle, A., Sivanesan, D., Hoeppner, S., and Baron, C. (2005) The putative lytic transglycosylase VirB1 from *Brucella suis* interacts with the type IV secretion system core components VirB8, VirB9 and VirB11. *Microbiology 151*, 3469–3482.
62. Carter, D. M., Miousse, I. R., Gagnon, J. N., Martinez, E., Clements, A., Lee, J., Hancock, M. A., Gagnon, H., Pawelek, P. D., and Coulton, J. W. (2006) Interactions between TonB from *Escherichia coli* and the periplasmic protein FhuD. *J. Biol. Chem. 281*, 35413–35424.
63. de Paz, H. D., Sangari, F. J., Bolland, S., Garcia-Lobo, J. M., Dehio, C., de la Cruz, F., and Llosa, M. (2005) Functional interactions between type IV secretion systems involved in DNA transfer and virulence. *Microbiology 151*, 3505–3516.
64. Bayliss, R., Harris, R., Coutte, L., Monier, A., Fronzes, R., Christie, P. J., Driscoll, P. C., and Waksman, G. (2007) NMR structure of a complex between the VirB9/VirB7 interaction domains of the pKM101 type IV secretion system. *Proc. Natl. Acad. Sci. U.S.A. 104*, 1673–1678.
65. Zhou, X. R., and Christie, P. J. (1997) Suppression of mutant phenotypes of the *Agrobacterium tumefaciens* VirB11 ATPase by overproduction of VirB proteins. *J. Bacteriol. 179*, 5835–5842.
66. Banta, L. M., Bohne, J., Lovejoy, S. D., and Dostal, K. (1998) Stability of the *Agrobacterium tumefaciens* VirB10 protein is modulated by growth temperature and periplasmic osmoadaption. *J. Bacteriol. 180*, 6597–6606.